Uncovering the magnetic properties of the $\mathbf{Ag}_x\mathbf{Ni}_y$ $(x + y = 55)$ nanoalloys in the whole composition range

R. H. Aguilera-del-Toro,[1,2] P.G Alvarado-Leyva,[3] and A. Vega[2]

[1]*Instituto de Física, Universidad Autónoma de San Luis Potosí, San Luis Potosí, México*

[2]*Departamento de Física Teórica, Atómica y Óptica, Universidad de Valladolid, Spain*

[3]*Facultad de Ciencias, Universidad Autónoma de San Luis Potosí, San Luis Potosí, México*

(Dated: October 4, 2018)

Abstract

Nickel and silver are metals with interesting properties of technological relevance: nickel is a well known ferromagnet and silver has antibacterial properties. Both exist in the face centered cubic phase but are immiscible. In the context of alloys at the nanoscale, one can play with the size to fine tune a desired property, or to achieve new properties and functionalities that do not exist at the macroscopic regime. In this work, we explore how the subtle interaction between Ni and Ag triggers the chemical order, the electronic structure, and the magnetic properties of a AgNi nanoalloy of 55 atoms, a size that can accommodate core/shell configurations with sizable parts. Calculations are conducted within the density functional theory at the generalized gradient approximation for exchange and correlation. We determine, in the whole composition range, the chemical order, absolute and relative stabilities by means of binding energy, excess energy and second energy difference, as well as total and part-projected spin-polarized electronic densities of states and local charge and spin magnetic moments distribution. Ni-core/Ag-shell structures are particularly stable, but contrary to what one would expect by simply extrapolating the properties of the pure Ag and Ni clusters or of pure fcc bulks, we find unexpected behaviors along the composition range, such as quenched magnetic moments in Ni, total magnetic moments essentially contributed in some cases by Ag, or electronic charge transfer that changes its sign depending on the stoichiometry. These behaviors lead to magnetic transitions as a function of the composition, and differ, in some cases, from those of the smaller 13-atoms AgNi nanoalloys of the same symmetry with which we compare, a further demonstration of the complex nature of nanostructures. The above trends are robust against ionization and electron capture.

PACS numbers: 75.75+a; 36.40Cg; 75.30.Pd; 75.50.-y

Keywords: nanoalloys, nanomagnetism, density functional theory, electronic structure

I. INTRODUCTION

One of the most interesting and long-standing research field in Materials Science is the design and characterization of alloys, and the seek of new routes to improve their properties in order to make them more efficient for specific purposes. Taking advantage of the cooperative effects of the constituent elements, one can envisage a large variety of applications depending on the composition and stoichiometry. Perhaps the most well known example is the combination of Fe and Cr to create stainless steel, whose properties can even be improved by the addition of other elements. At present, we have already collected a large amount of thermodynamic data, such as binary and ternary phase diagrams, chemical compositions and crystalline structures[1] and we understand the physical and chemical properties of many alloys[2]. In the macroscopic regime, one can play with the constituent elements, stoichiometry and growth conditions in order to create alloys with specific properties. For example, Mpourmpakis *et al.* studied Fe-Co in bulk regime[3] and they found that alloys with Co concentration of 30% were those having the highest magnetic moment. However, the physical and chemical properties of a material can be drastically modified at the nanoscale, as a consequence of quantum-confinement effects, and this is why nanoparticle research has become such a fascinating branch of Material Science. Therefore, in the context of alloys at the nanoscale, one can also play with the size as a new degree of freedom to fine tune a desired property, or to achieve new properties and functionalities that do not exist at the macroscopic regime.

The often unexpected and difficult to rationalize behavior of nanoalloys poses a great challenge, but at the same time is a breeding ground for surprising discoveries and innovative technological applications[4,5]. An intense effort has been devoted in the last years to investigate different kinds of nanoalloys, but the collected data is still scarce in comparison with what we have for macroscopic alloys. It is well known now that the most stable stoichiometries and chemical orders of nanoalloys do not correspond, in general, with those of their macroscopic counterparts. The relative position of the different atoms in a nanoalloy of a given composition leads to a large number of homotops that correspond to different chemical orders. Therefore, from a theoretical point of view, the determination of the low-energy isomers is a challenging task[6]. In the case of magnetic nanoparticles, the low-energy spin states (spin isomers) have to be also characterized. In some cases, structure, chemical

order and spin configuration are competitive from the energetic point of view. Bimetallic nanoparticles, made up of atoms of two different chemical species, are the simplest kind of nanoalloys.

At the macroscopic level, Ni and Ag are known to be inmiscible for all compositions[1]. Annealing studies of Ni/Ag films also show clustering of Ni atoms to form Ni nanoparticles embedded in a Ag matrix, a similar trend as that observed in chemically similar CoAg films[7]. Ni belongs to the ferromagnetic elements of the 3d series, and pure Ni nanoparticles have been extensively studied due to their magnetic properties which make them good candidates for their use in high density magnetic recording devices[8,9] . The unavoidable oxidation in environmental conditions, however, reduces in general their magnetic moment due to the appearance of antiparallel magnetic couplings[10–15]. Ag nanoparticles have been shown to exhibit antibacterial properties[16–18]. The Ag-Ni system has been synthesized by several methods, such as laser-liquid-solid interaction technique[19], by laser induced plasma[20] and borohydride reduction method[21]. Synthesis methods have been also developed for tecnological applications such as sensors[22], and for enhancement of photo catalytic activity[23]. Through Raman diffusion at low frequency, Portales *et al.* found core-shell structures for NiAg nanoparticles[24], in which Ni atoms form the core and Ag the shell, with a weak bonding between the Ni and Ag atoms. The segregation is driven by the lower surface energy of Ag and the large size mismatch (the Ni atomic radii is 1.25Å, and that of Ag 1.45Å). This segregation was also observed by Gaudry *et al.* in $Ni_{0.5}Ag_{0.5}$ nanoparticles[25]. Recent simulations[26,27] further showed the tendency of NiAg nanosystems to form core-shell structures. In those studies, global optimizations with a empirical Gupta potential, were performed for NiAg clusters with 34 and 38 atoms for all possible compositions. For fixed size and variable composition, perfect core-shell structures turned out to be the most stable chemical orders, in qualitative agreement with the experimental findings. Calvo *et al.*[28] have demonstrated through Montecarlo simulations, that the core/shell configuration is stable up to 810K. The empirical approach with the Gupta potential, relies on structural parameters, so that electronic effects that could drive the stabilization of certain structures or homotops, or that could be essential for certain properties, are not taken into account, in contrast to a DFT approach. Although systems with a large number of atoms can be investigated with low computational cost, the description of the energy landscape provided by the empirical approach is less accurate than that provided by a DFT approach, although a good sampling

can be achieved.

The icosahedral Ag-Ni nanoalloy of 13 atoms was studied by Harb and co-workers[29] using density functional theory. In a similar work, Harb et al[30] studied the smaller nanoalloys Ag_nNi_p with $n + p \leq 6$. They found that Ni atoms are brought together maximizing the number of Ni-Ni bonds, and that the Ag atoms are located around a Ni subcluster maximizing the number of Ag-Ni bonds. They found a very important contribution of the d-electrons of silver atoms located at surface in the optical response of the system. Those small 13-atoms nanoalloys, however, can not accommodate a core/shell structure with a core of more than one atom. All the above studies point to the possibility of designing magnetic NiAg nanoalloys in which the magnetic moment of Ni could be protected in environmental conditions (against oxidation for instance), or other environments like those existing in the human body. At the same time, the Ag content should provide a functionalization of such nanoparticles with antibacterial properties, which would broaden their range of applications.

The aim of the present work is to characterize, in the framework of the density functional theory, the chemical order, electronic structure, and related properties like structural parameters, thermodynamical stability, relative stoichiometric stability and magnetism, of Ag_xNi_y icosahedral nanoalloys of 55 atoms, in which core/shell structures with sizable Ni subclusters can be achieved along the composition range. Pure Ag_{55} and Ni_{55}, that are the limits of compositions, have been shown to stabilize in the icosahedral ground state[31–33], contrary to what happens in the smaller nanoalloy of 13 atoms for which Pereiro and co-workers found the icosahedron as the global minimum energy[34], whereas Fernández et al, found a BBP-like structure[35]. **The size of this 55-atoms nanoalloy is, on the other hand, closer to what can be experimentally attained. For simplicity, we assume the Mackay icosahedral structure along the full composition range. Although icosahedral structures are more plausible in the 55-atoms nanoalloy than in the 13-atoms one, we note that due to the large Ag and Ni size mismatch and resulting stress, poli-icosahedral structures, irregular or antimackay icosahedral structures could appear at intermediate sizes instead of Mackay ones. These facts have been already shown for NiAg nanoalloys, mostly for larger ones where quiral shells can be also formed[26,36–38]**. We have considered all possible homotops, as well as the different spin isomers, so that metastable chemical orders and spin excitations are also characterized. We complement our investigation with the study of the effects of an electron deficit or excess,

which is important upon ionization or electron capture.

The paper is organized as follows. In Sec. II, we describe the theoretical and computational approach. In section III are discussed the stability, chemical order, structural parameters and electronic structure; section IV is devoted to the magnetic properties. The conclusions are summarized in the last section.

II. THEORETICAL APPROACH AND COMPUTATIONAL DETAILS

We performed fully self-consistent DFT calculations using the SIESTA code[39], an efficient DFT implementation that solves the spin-polarized Kohn-Sham equations within the pseudopotential approach to treat the core interactions, and employs numerical pseudoatomic orbitals in the basis set. For the exchange and correlation potential we used the Perdew-Burke-Ernzerhof form of the generalized gradient approximation (GGA).[40] We employed norm-conserving scalar relativistic pseudopotentials[41] in their fully nonlocal form[42], generated from the atomic valence configuration $3d^8 4s^2$ for Ni (with core radii 2.00, 2.44 and 2.50 a.u. for s, p and d orbitals, respectively), and $4d^{10}5s^1$ for Ag (with core radii 2.17, 2.82 and 2.40 a.u. for s, p and d orbitals, respectively) Non-linear partial core corrections[43], which are known to be important for transition metal pseudopotentials, are included at the core radius of 0.7 Å. Valence states were described using double-ζ basis sets for Ni and Ag, with maximum cutoff radii of 4.931 Å ($2p$) and 7.998 Å ($3d, 4s$), respectively. A $4p$ polarization orbital was also considered for Ni, with cutoff radius 7.998 Å6.599 Åfor nickel an silver respectively. The energy cutoff used to define the real-space grid for numerical calculations involving the electron density was 250 Ry. The Fermi distribution function that enters in the calculation of the density matrix was smoothed with an electronic temperature of 15 meV. We used an energy criterium of 10^{-4} eV for converging the electronic density. In the calculations, the individual clusters were placed in a cubic supercell of $20 \times 20 \times 20$ Å^3, a size large enough to neglect the interaction between the cluster and its replicas in neighboring cells. It was considered only the Γ point ($k = 0$) when integrating over the Brillouin zone, as usual for finite systems.

The equilibrium geometries resulted from an unconstrained conjugate-gradient structural relaxation using the DFT forces. Icosahedral structures are considered. We relaxed each homotop and spin state until interatomic forces were smaller than 0.001 eV/Å. In all cases,

different spin isomers were checked in order to ensure the correct ground state. The strategy for sampling the chemical orders was as follows. First of all, we took advantage of the symmetries to define those inequivalent positions of the Ni and Ag atoms for each composition; this reduces the number of homotops to calculate. Then, by selecting pertinent minimal sets of homotops, we determined general trends that allowed us to exclude certain kind of chemical orders and several of their corresponding homotops. In particular, we determined the preference of Ni atoms to occupy central sites, as well as to form Ni subclusters within the system.

As a first step, we calculated the AgNi nanoalloy of 13 atoms with icosahedral structure for two purposes. One was to benchmark our theoretical approach against previous results for the same system in the Ag rich phase by Harb and co-workers[29] using the Gaussian code with GGA-PB86 and LANL2DZ relativistic effective core potential. In the supplementary information (SI) we provide several low-energy homotops. The second purpose of this calculation was to have a reference to compare with the 13-atoms core of the larger 55-atoms nanoalloy with compositions up to 13 Ni atoms, in order to assess the role played by the interaction with the remaining 42 Ag atoms at the shell. This will be discussed in the following sections. Our ground states (see the SI) are the same as theirs, except for $Ag_{10}Ni_3$, for which our predicted ground state corresponds to their first isomer (nearly degenerated with the ground state). We complete the study of the AgNi nanoalloy of 13 atoms to cover all the composition range, not reported so far. For selected compositions or homotops for which we found different states very close in energy, or untypical magnetic arrangements, additional calculations were performed using the VASP code[44,45] with the same GGA functional as that employed in SIESTA. VASP solves the Khon-Sham equations using a plane-waves basis set instead of numerical pseudoatomic orbitals, and the core interactions are treated be means of the projector-augmented wave (PAW) approach instead of pseudopotentials. This approach is consistent with the exact all-electron potential and provides a more accurate description of the core interactions. However, VASP is more demanding than SIESTA from the computational point of view. In all cases tested, VASP and SIESTA yielded similar results. A comparison of the magnetic moment obtained from both approaches in three of those selected compositions of the 13-atoms nanoalloy can be found in the SI. The local electronic charge and magnetic moments distribution within the nanoalloys were determined from the Mulliken population (see the SI), although in those same cases where additional

VASP calculations were conducted, we performed this analysis using Bader's method[46,47] which divides the nanoalloy into atomic volumes by locating the zero-flux surfaces of the electron density field.

III. CHEMICAL ORDER, STABILITY AND ELECTRONIC PROPERTIES

The ground state configurations of Ag_xNi_y $(x+y=55)$ nanoalloys are shown in Fig.1. In the SI, the reader can find several low-energy homotops for each composition, corresponding to metastable chemical orders. Regarding the inter-atomic distances of the nanoalloys, we find that Ni-Ni bonds are shorter than Ag-Ni bonds, and these are shorter than Ag-Ag ones. The average inter-atomic distances remain almost constant as a function of stoichiometry (2.75 Å for Ag-Ag, 2.65 Å for Ag-Ni, and 2.46 Å for Ni-Ni). An electron excess or deficit does not modify the chemical order, since the corresponding ground state homotops are the same as in the neutral nanoalloy. The chemical order pattern is clear. Ni atoms tend to occupy the internal positions, building up a Ni subcluster. This is consistent the lower atomic volume and the larger cohesive energy of Ni as compared to Ag. The lower average inter-atomic distances in Ni_{55} than in Ag_{55} creates a size mismatch when the nanoalloy is formed, causing a steric effect that tends to favor segregation of the bigger atomic species (Ag) to the surface positions. The larger cohesive energy of Ni as compared to Ag favor segregation of Ni to the interior positions so that a larger number of the more cohesive Ni-Ni bonds can be generated. Therefore, segregation always occurs, and a core/shell structure tends to be formed, in agreement with the experimental findings[24,25] and calculations of smaller AgNi nanoalloys[26,27,29,30] **and larger ones[36–38].** When the number of Ni atoms is lower than 14, all them occupy the most internal positions. $Ag_{42}Ni_{13}$ is a perfect core/shell cluster, and the next Ni atom in $Ag_{41}Ni_{14}$ starts occupying the outer shell of the 55-atoms icosahedral structure in positions as close as possible to the already formed Ni_{13} core. The chemical order pattern is, thus, the one that maximizes the number of Ni-Ni bonds with a Ni subcluster surrounded by Ag atoms. The robustness of this chemical order pattern is demonstrated by the fact that for all 55-atoms nanoalloys with less that 14 Ni atoms, except $Ag_{52}Ni_3$ and $Ag_{48}Ni_7$, their 13-atoms core has the same chemical order (corresponds to the same homotop) as the ground state of the 13 atoms nanoalloy of the corresponding stoichiometry. This also points to the fact that the outer 42 Ag atoms may provide protection to the core. We will

come to this point later. **Another result showing the robustness of the described chemical order pattern is that the $Ag_{12}Ni_{43}$ homotop with the 12 Ag atom at the 12 vertices of the shell results 1.8 eV less stable than the putative ground state (both fully relaxed). The high cohesive energy of Ni favors the Ni-Ni bonds, as discussed above. On the other hand, this result could be seen, in some sense, as a manifestation of the tendency to off-center cores as increasing the core size[37]** We calculated the second energy difference ($\Delta_2 E$) to determine the relative stabilities of the different stoichiometries with respect to their neighboring ones. This magnitude is defined as follows:

$$\Delta_2 E(x,y)^{0/\pm} = E(x+1,y-1)^{0/\pm} + E(x-1,y+1)^{0/\pm} - 2 \times E(x,y)^{0/\pm}$$

In order to compare the nanoalloy with an ideal mixture of the pure clusters, we evaluated the excess energy (E_{exc})[48]

$$E_{exc}(x,y) = E(x,y) - x\frac{E(\mathrm{Ag}_{x+y})}{x+y} - y\frac{E(\mathrm{Ni}_{x+y})}{x+y}$$

where $E(\mathrm{Ag}_{x+y})$ and $E(\mathrm{Ni}_{x+y})$ are the energies of the pure clusters in their ground states. A negative excess energy indicates that formation of the corresponding nanoalloy is energetically favorable as compared to an ideal mixture. The ideal mixture would follow a simple Vegard law, according to which the total energy of the nanoalloys follows a linear behavior connecting the energies of the pure clusters. Fig.2 collects the data of $\Delta_2 E$ and E_{exc} for the different stoichiometries. The excess energy (Fig.2 upper panel) shows that, although all the nanoalloys are stable, according to their binding energy (given in the SI), only the formation of few of them, corresponding to certain stoichiometries with less than 14 Ni atoms, is favourable with respect to an ideal mixing of Ag_{55} and Ni_{55}, reflecting the strong tendency to segregation, instead of to maximize the number of Ni-Ag bonds. In all those stoichiometries, the Ni subcluster is completely covered by Ag. E_{exc} exhibits marked minima for $Ag_{54}Ni$, $Ag_{48}Ni_7$, $Ag_{42}Ni_{13}$, $Ag_{26}Ni_{29}$, $Ag_{23}Ni_{32}$. The first one, $Ag_{54}Ni$, corresponds to the smallest perfect core/shell configuration with the Ni atom in the center of the 55-atoms icosahedron.

$Ag_{42}Ni_{13}$ is the next perfect core/shell structure with a perfect 13-atoms Ni core. This is the most representative perfect core/shell Ni@Ag nanoparticle with both core and shell of considerable size, and will be analyzed in more detail later. The other three correspond to very symmetrical arrangements. $Ag_{48}Ni_7$ has a decahedral nickel subcluster, which is a closed structure, forming a quasi perfect core/shell structure. In $Ag_{26}Ni_{29}$ and $Ag_{23}Ni_{32}$, the nickel sub-cluster has an almost closed structure, with a mushroom-like structure. The second energy difference (Fig.2 lower panel) shows marked peaks at exactly the same stoichiometries, which is an indicator of their relative stability with respect to neighboring stoichiometries, and of their abundance if grown from their constituent atoms in a thermodynamical bath. Those stoichiometries can be considered as magic compositions for this nanoalloy. Besides, all except $Ag_{48}Ni_7$ remain magic compositions upon ionization or electron capture. $Ag_{48}Ni_7$ has no peak of $\Delta_2 E$ in the anionic state, being the peak shifted to $Ag_{47}Ni_8$. The highest peak of $\Delta_2 E$ corresponds to $Ag_{54}Ni$ (the first core/shell structure). We note that among the smaller 13-atoms nanoalloys, $Ag_{12}Ni$ with a central Ni atom gives the highest peak in $\Delta_2 E$, reflecting the high relative stability of this arrangement also in the smaller nanoalloy. **The reason of the high stability of $Ag_{54}Ni$ in the Mackay icosahedral structure has been already analyzed by Mottet et al.[49] who also shown that in the icosahedral Ag_{55} cluster, the single impurity of Ni located at the central site even increases the melting temperature. As these authors point out, the icosahedral structure results more stable in these clusters than a crystal fragment because it optimizes the surface energy (more compact facets are exposed at the surface in an icosahedron). However, the strong distortion produced of the lattice creates strain and compression at the center of the icosahedron because inter-shell distances are contracted. Introducing a smaller atom (like Ni) at the central site of the icosahedron relaxes this strain thus reducing the compression at the center. Therefore, from the energetic point of view, the central site is the optimal position for the Ni impurity.** It is interesting to analyze how the Ag-Ni hybridization evolves as varying the Ag/Ni ratio starting from one of the stoichiometric limits. In the SI are collected the total and element-projected density of electronic states (DOS), as going from $Ag_{54}Ni$ to $AgNi_{54}$. The overall shape of the DOS is similar, provided that the atomic arrangement is icosahedral in all cases, and that at this Ni concentration regime all the nanoalloys are in low-spin states as we will discuss in the next section (we will see that in

the high Ni-concentration the nanoalloys are, on the contrary, strongly spin-polarized and sustain a considerable magnetic moment). The Ag-Ni hybridization takes place close to the Fermi energy, down to 2 eV below E_F, being the lower energy states essentially contributed by Ag. The HOMO progressively acquires Ni character as increasing the Ni content, reaching the nearly pure Ni character already at a low Ni content. The Ni character of the HOMO, even for those nanoalloys for which all Ni atoms are located in a core surrounded by Ag indicates that, although the Ag-Ni is relatively weak and Ag provides physical protection to the core, Ni states should play an important role in the reactivity of these nanoalloys, as well as in other processes like ionization. Thus, upon ionization, the electron is mainly extracted from the Ni states. Other electronic properties like the adiabatic ionization potential and electron affinity of both the ground state and low-energy homotops of these nanoalloys can be found in the SI.

IV. MAGNETIC PROPERTIES

The total spin magnetic moment of the predicted ground states of the 55-atoms AgNi nanoalloys is plotted in Fig.3 in the whole composition range. Several magnetic phase transitions take place. Let us focus first on the neutral nanoalloys, starting from the low Ni concentration limit. We note that small pure Ag clusters can sustain a magnetic moment in contrast to the Ag bulk; Ag_{55} is in a low spin state ($3\mu_B$) while Ni_{55} is in a high spin state ($40\mu_B$) characterized by parallel magnetic couplings (reminiscent from the ferromagnetic Ni fcc) and per atom magnetic moment of $0.7\mu_B$/atom (slightly larger than that in the bulk). $Ag_{54}Ni$ is the first perfect core/shell cluster with the Ni atom in the center. The moment of $Ag_{54}Ni$ is $4\mu_B$, that is one μ_B larger than that of Ag_{55}, although this increase is, unexpectedly, contributed by the Ag atoms and not by the Ni one. Fig.4 shows the local charge and magnetic moment distribution in this cluster. An electronic charge transfer from the outer 42-atoms to the inner 13-atoms takes place. This is a general trend in the 55-atoms nanoalloy (see the SI for other stoichiometries). The Ni atom gains 0.35 electrons and its moment is quenched ($0.08\mu_B$) and antiparallel to those of Ag. **The quenching of the magnetic moment in the Ni atom is consistent with the loss of the moment in magnetic impurities embedded in a nonmagnetic matrix. The reason is the electron delocalization and hibridization with the host states, as ilustrated in the**

DOS shown in the SI and manifested by the noticeable electronic charge gained by the Ni atom due to charge transfer from Ag. We note that in a system with more than half-band filling (like Ni) an increase of charge tends, in general, to reduce the spin-polarization. Therefore the magnetic moment of this cluster is esentially contributed by the Ag atoms, and in particular by those located at the surface shell. The 42-atoms outer shell of Ag plays here an important role that can be assessed by comparing the local charge and moment distribution in the inner 13-atoms core of $Ag_{54}Ni$ (Fig.4) with the distribution in the smaller $Ag_{12}Ni$ nanoalloy (in the SI).

In Fig.5 we plot the total magnetic moment of the 55-atoms AgNi nanoalloys for compositions up to $Ag_{42}Ni_{13}$ together with that of the 13-atoms AgNi nanoalloy for the sake of comparison. We also separate, in the case of the 55-atoms nanoalloy, the contributions of the 42 outer atoms and of the 13 inner ones (the local charge and moment distribution in the 13-atoms AgNi nanoalloys of different compositions can be found in the SI). Despite the fact that $Ag_{12}Ni$ has $4\mu_B$ like $Ag_{54}Ni$, the Ni atom contributes $0.65\mu_B$ in the smaller 13-atoms cluster. In contrast, the inner 13 atoms of $Ag_{54}Ni$ contribute together less than $0.5\mu_B$ to the total moment. The outer Ag atoms lose charge in favor of the central Ni atom. Therefore, the spin-polarized electronic charge distribution within the 13 atoms cluster dramatically changes upon its capping with the 42 Ag atoms of the outer shell, and this holds along the low Ni content regime of the nanoalloys. The charge transfer is triggered by the atomic environment to a large extent. We note that although the electronegativities of Ag and Ni are similar, in the 55 atoms nanoalloy with less than 14 Ni atoms, the charge transfer takes place from the outer Ag atoms to all the inner 13 ones, included the Ag inner atoms. However, in the smaller 13 atoms nanoalloy, no Ag atom gains electronic charge.

Contrary to what one would expect based on an extrapolation between the values of the magnetic moments of the pure Ag_{55} and Ni_{55} clusters, the total moment of the nanoalloy in the high Ag concentration limit decreases as increasing Ni concentration up to $Ag_{50}Ni_5$, an exception being the discussed $Ag_{54}Ni$ case. Up to $Ag_{50}Ni_5$, the inner 13 atoms contribute less than $1\mu_B$, the decrease in the total moment being, therefore, due to a decrease in the spin-polarization of Ag. The lowest moment (singlet state) is reached at $Ag_{50}Ni_5$ in which the spin polarization is completely quenched. We note that the singlet state here is due to antiparallel magnetic couplings and low local magnetic moments (see Fig.6). An interesting magnetic trend concerns the coupling between Ni atoms when the Ni subcluster is small.

This coupling is sensitive to the atomic environment and to the interaction with Ag. We have already seen in the previous paragraph that when a Ni subcluster of less than 6 atoms is covered by Ag in the 55-atoms nanoalloy, the Ni moment is quenched. If we compare the magnetic couplings of the Ni subclusters (up to 13 Ni atoms) in the 55-atoms with the 13-atoms nanoalloys, we find that in the absence of the 42 Ag atoms of the shell, few Ag atoms in the smaller nanoalloy are enough to promote antiparallel couplings between Ni atoms. Even one Ag atom in the $AgNi_{12}$ nanoalloy promotes antiparallel couplings within the Ni subcluster. In general, The same Ni subclusters that were magnetically quenched in the 55-atoms nanoalloy, but preserving parallel couplings, have antiparallel magnetic couplings in the 13-atoms nanoalloy, which lead to an unusual and unexpected magnetic arrangement for a system made of a late transition metal element like Ni, and it is a manifestation of the complex and rich magnetic arrangements that can be found at the nanoscale, depending on the size, and on the atomic and chemical environments. **In this composition range, the Ni subcluster is very small, and due to the high average Ni-Ag coordination and corresponding strong Ni-Ag hybridization (see the DOS in the SI) and noticeable charge transfer, the spin polarization is strongly reduced (although not as much as in the single embedded impurity). Consequently, the Ni-Ni bonding weakens and the tendency to develop parallel magnetic couplings characteristic of pure Ni systems decreases. A manifestation of the weakening of the Ni-Ni bonding is the large average Ni-Ni interatomic distance in the Ni subcluster, particularly in the low Ni concentration regime. This distance is larger than that of the relaxed freestanding Ni cluster extracted from the nanoalloy. The Ni dimer in Ag53Ni2 has an interatomic distance that exceeds in 20% that of the free-standing Ni_2. As soon as the Ni content exceeds a critical value, and a sufficiently big Ni core is formed, this distance tends to equal the one in the pure Ni cluster, but the increase is still noticeable up to $Ag_{45}Ni_{10}$ where the Ni subcluster is still expanded by about 7%. Further support to the assesment that Ni-Ag hybridization and charge transfer is fundamental in governing the magnetic properties here is the fact that a pure Ni cluster has larger magnetic moments if it is expanded. We have checked this in our case by repeating calculations for several Ni subclusters extracted from the nanoalloy.**

Beyond this Ni concentration ($Ag_{50}Ni_5$) the total moment linearly increases as increasing

the Ni content, with a sudden drop of $9\mu_B$ at $Ag_{18}Ni_{37}$, to continue the linear increase with the same slope as before till the pure Ni_{55} limit. The linear increase is associated with the formation of a compact Ni subcluster with a net magnetic moment that contributes most of the moment of the nanoalloy in this composition regime. Fig.6 shows that beyond $Ag_{50}Ni_5$, the moment of the inner 13 atoms of the nanoalloy is now similar to the moment of the 13-atoms nanoalloy of the corresponding stoichiometry, and that the contribution of the outer 42-atoms shell becomes negligible, although it points in the same direction as the Ni moment (this Ag-Ni coupling holds for larger Ni content until the sudden drop at $Ag_{18}Ni_{37}$ occurs). The above results demonstrate that the formation of a sizable Ni subcluster allows it to preserve its magnetic identity to a large extent when covered or interfaced by Ag, with a weak core-shell interaction, and that the magnetic moment of the nanoalloy is, thus, localized in the Ni subcluster. In the previous section, we have discussed how the electronic density of states evolves as increasing the Ni content in the nanoalloy, and how the increase in the total moment is consistent with the enhancement of the spin-polarization of the molecular orbitals with most Ni character, which are those located close to E_F. The magnetic ordering in Ni is parallel, in contrast with the few antiparallel couplings of the smaller 13-atoms nanoalloy (see Fig.2 in the SI).

At the stoichiometry $Ag_{18}Ni_{37}$, the nanoalloy reaches a total moment of $32\mu_B$, with per Ni-atom moment of $0.85\mu_B$. This spin polarization in Ni exceeds by 30% the one in the Ni fcc bulk. It is expected that as increasing the size of a Ni cluster its magnetic moment converges to the bulk value. The sudden drop of the magnetic moment occurring at $Ag_{18}Ni_{37}$ is mainly due to a reduction of the spin polarization in the Ni subcluster while keeping the parallel magnetic couplings reminiscent of the ferromagnetic order of the bulk. Beyond this magnetic phase transition, the rather small moment of Ag points in opposite direction to the Ni moment, but it is negligible. This drop of spin polarization in Ni ensures a per atom magnetic moment in Ni_{55} similar to the bulk one. The mentioned antiparallel coupling between the magnetic moments of Ag and Ni is also found in the 13-atoms nanoalloy, particularly in the rich Ni regime. We also also that the total magnetic moment of a 55 atoms nanoalloy with a given composition is more robust against the chemical order than that of the 13-atoms nanoalloy. This can be inferred by comparing the magnetic moment of the low-energy homotops in the nanoalloys of both sizes.

The rest of this section is devoted to the analysis of the other perfect core/shell cluster,

$Ag_{42}Ni_{13}$ with a 13-atoms icosahedral Ni core. This 55-atoms core/shell cluster has $8\mu_B$, exactly the same as Ni_{13}, most of which ($7.42\mu_B$) is localized in the Ni core. This situation is also present in CoCu and CoAu nanoalloys, where Co atoms are totally covered by Cu and Au atoms respectively.[50] Fig.7 illustrates the local charge and magnetic moment distribution in this cluster. The central Ni atom loses 0.26 electrons, so that a radial oscillation of charge transfer takes place. This electronic deficit leads the inner atom to have a large moment of $0.94\mu_B$. The magnetic couplings are parallel. The density of states of $Ag_{42}Ni_{13}$ is plotted in the SI for the three charge states. The Ag and Ni contribution to the molecular orbitals along the spectrum in clear and illustrates a weak Ag-Ni interaction and a high spin-polarization, particularly in the states mostly contributed by Ni. The HOMO of the neutral cluster is of minority spin. This explains why upon ionization the magnetic moment increases $1\mu_B$ as shown in Fig.3 (the electron is extracted from minority spin states) while the opposite happens upon an electron capture. This is a general trend in most of the composition range except in the rich Ag limit (up to $Ag_{48}Ni_7$) where the above trend is reversed in several stoichiometries. The DOS of the neutral clusters in this region, plotted in the SI, do not allow such a clear interpretation; the HOMO character has also a large Ag contribution and the overall spin polarization is much weaker. We note that another exception to this rule can be found at the magnetic phase transition at $Ag_{18}Ni_{37}$ which, in the case of the cationic nanoalloys, occurs earlier (at $Ag_{20}Ni_{35}$ instead) and, consequently, in the intermediate concentrations the total moment changes upon ionization by $9\mu_B$. The drop in the cationic nanoalloys to restore the per atom moment in Ni occurs at a lower Ni content since ionization further increases the Ni moment as a consequence of the aforementioned spin- and element-character of the HOMO.

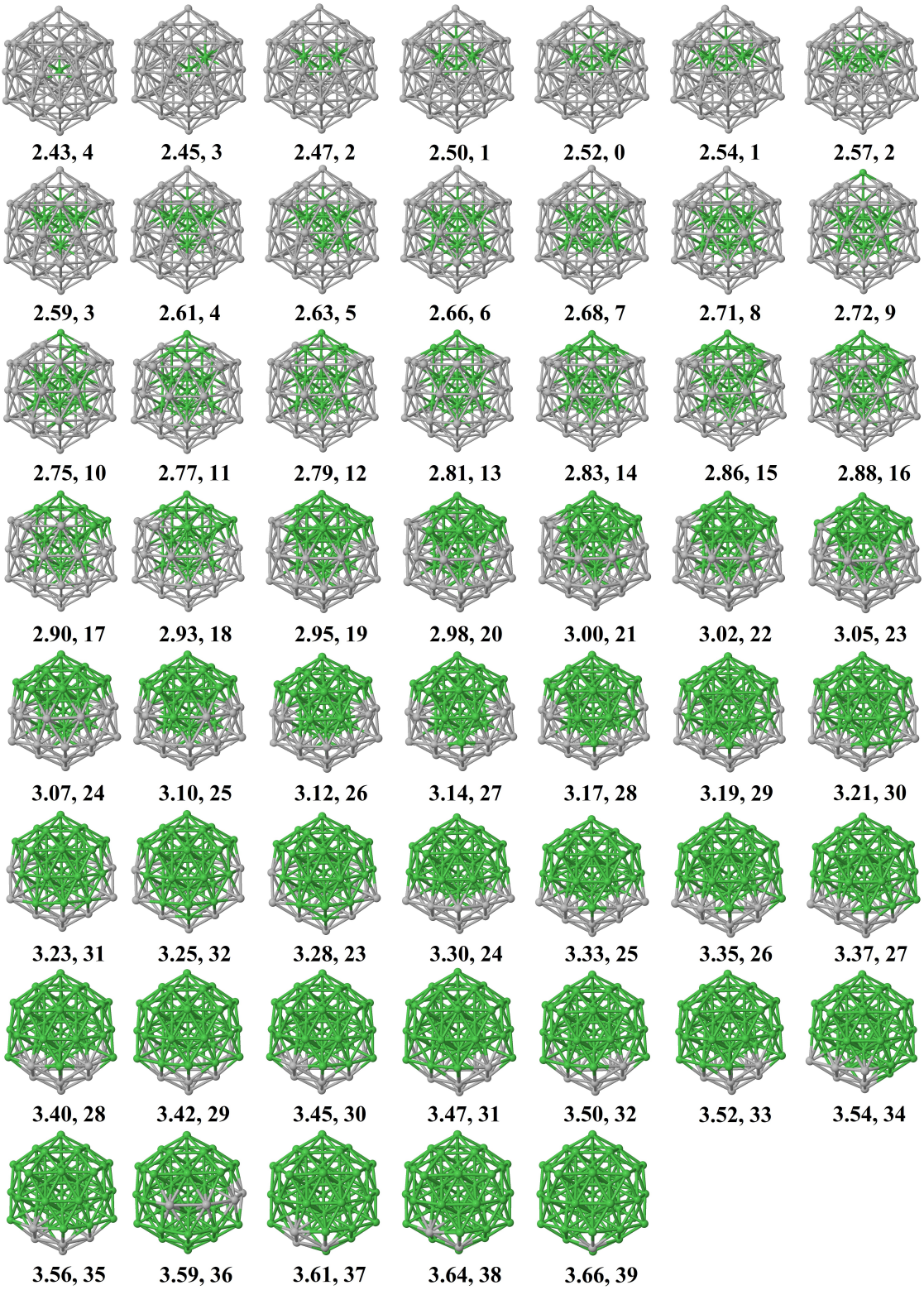

FIG. 1: (Color online) Ground state geometries of $[Ag_xNi_y]$ clusters with $x+y=55$. The numbers below the structures are the binding energy per atom (in eV) and the total spin magnetic moment (in μ_B), respectively.

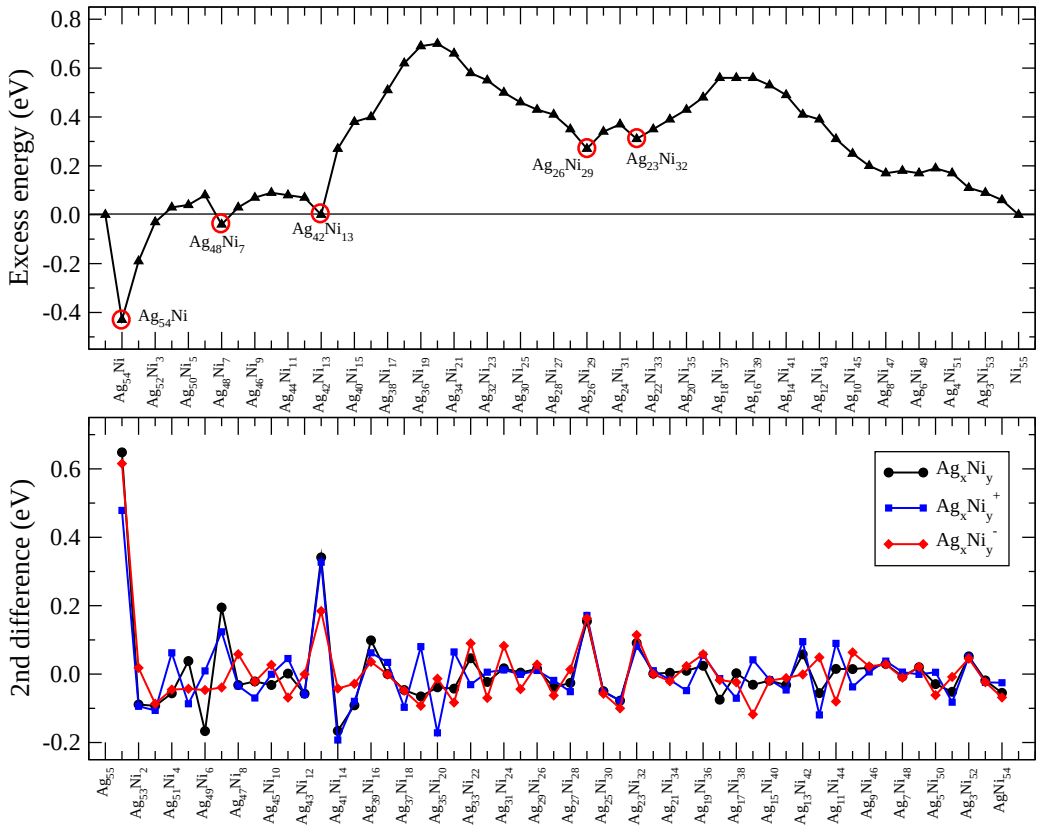

FIG. 2: (Color online) Excess energy (upper panel) and second energy difference (lower panel) of $[Ag_xNi_y]$ clusters with $x + y = 55$. The local minima of excess energy are highlighted.

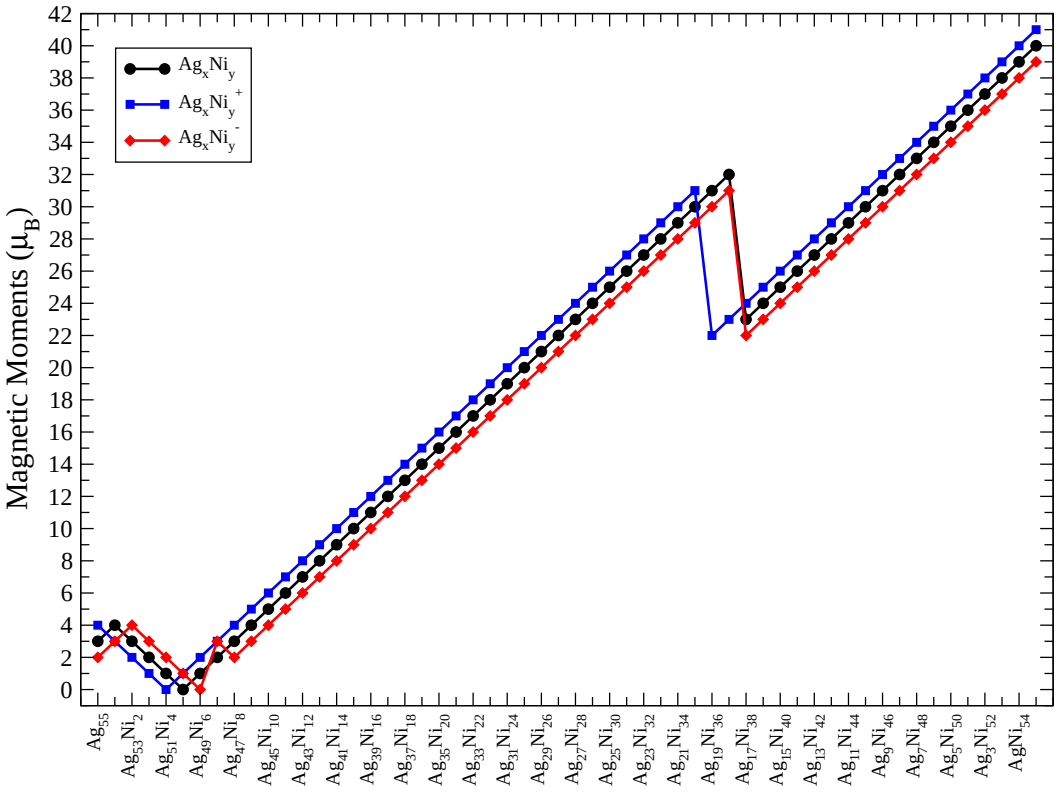

FIG. 3: (Color online) Total spin magnetic moment of the $[(Ag_xNi_y)^{0/\pm}]$ clusters with $x + y = 55$ as a function of the composition.

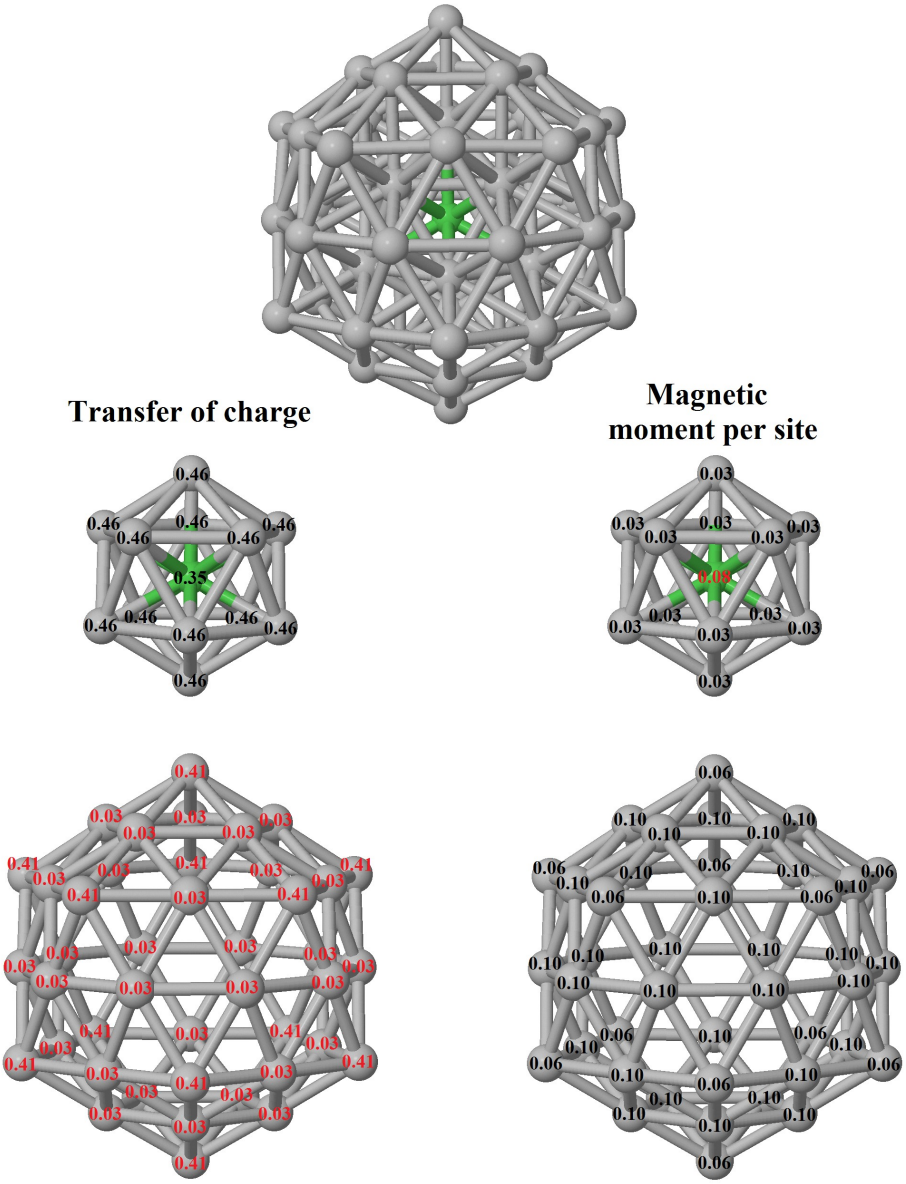

FIG. 4: (Color online) Local electronic charge transfer and magnetic moment of $Ag_{54}Ni$ cluster. For charge transfer, numbers in black (red) indicate gain (loss) of charge; for the magnetic moment, numbers in black (red) indicate spin up (down). Contributions of the inner 13 atoms and the outer 42 are separated for the sake of clarity.

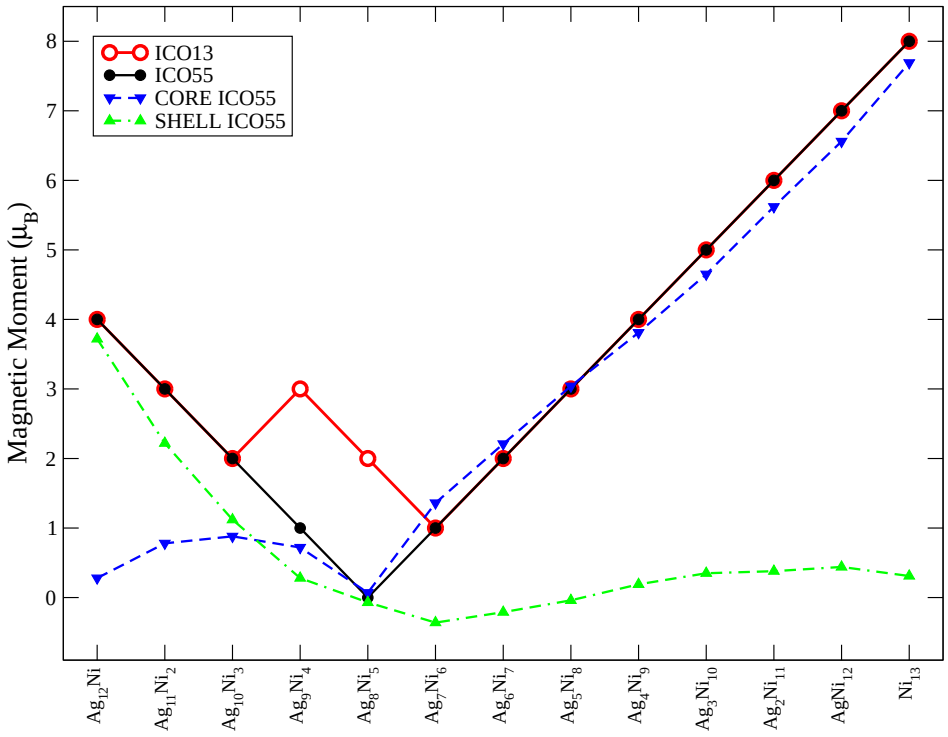

FIG. 5: (Color online) Total magnetic moment of the 55-atoms AgNi nanoalloys for compositions of Ni content up to $Ag_{42}Ni_{13}$ (black circles). Total magnetic moment of the 13-atoms AgNi nanoalloys in the whole composition range (open circles). Contribution of the 42 outer atoms (up green triangles) and of the 13 inner ones (down blue triangles) of the 55-atoms AgNi nanoalloys to their total moment.

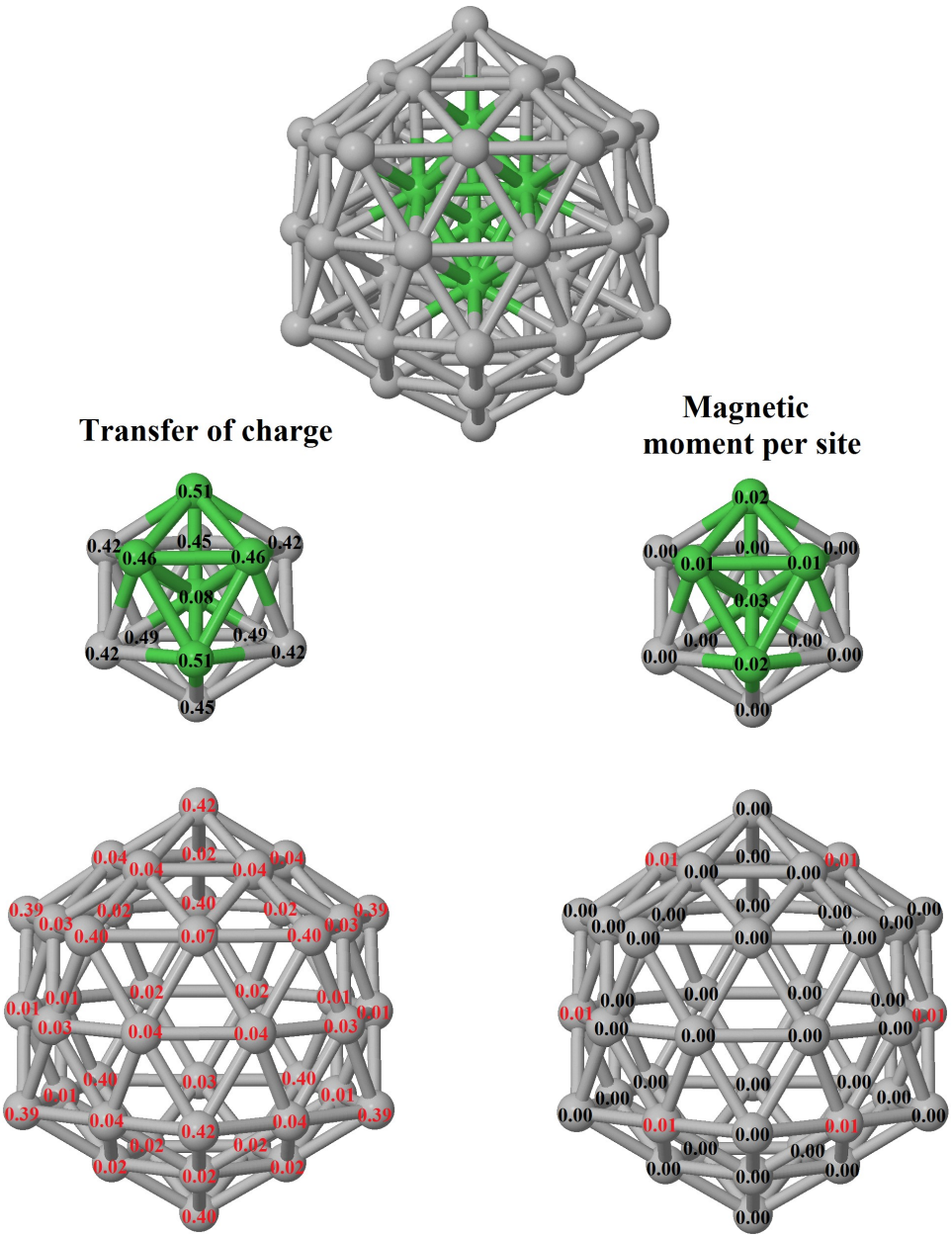

FIG. 6: (Color online) Local electronic charge transfer and magnetic moment of $Ag_{50}Ni_5$ cluster. For charge transfer, numbers in black (red) indicate gain (loss) of charge; for the magnetic moment, numbers in black (red) indicate spin up (down). Contributions of the inner 13 atoms and the outer 42 are separated for the sake of clarity.

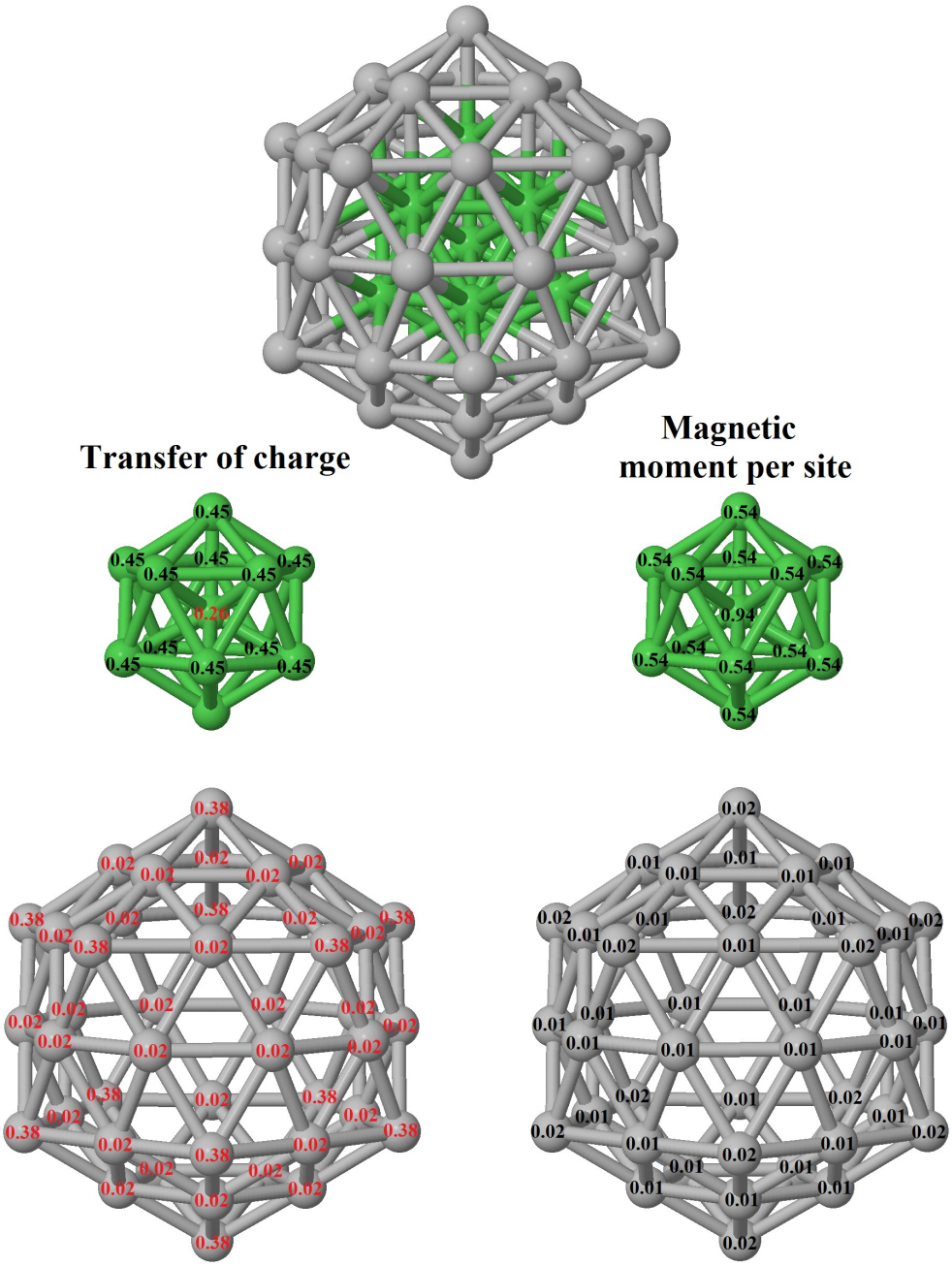

FIG. 7: (Color online) Local electronic charge transfer and magnetic moment of $Ag_{42}Ni_{13}$ cluster. For charge transfer, numbers in black (red) indicate gain (loss) of charge; for the magnetic moment, numbers in black (red) indicate spin up (down). Contributions of the inner 13 atoms and the outer 42 are separated for the sake of clarity.

Acknowledgments

This work was supported by the Spanish Ministry of Economy and Competitiveness (Project FIS2014-59279-P) in conjunction with the European Regional Development Fund (FEDER). P.G.A.L acknowledges to CONACyT for financial support through "Proyecto Apoyado por el Fondo Sectorial de Investigacion para la Educación" with reference number 237882. R.H.A-T acknowledges the fellowships from CONACyT (Mexico, scholarship 415121) and UVa (Universidad de Valladolid).

V. CONCLUSIONS

We investigated, using the density functional theory within the GGA approximation of Perdew-Burke-Ernzerhof, the energetic stability, chemical order, electronic structure, and magnetic properties, of Ag_xNi_y nanoalloys of 55 atoms with icosahedral shape. We also studied the effects of an electron deficit or excess.

Ni atoms tend to occupy the internal positions, building up a Ni subcluster, and developing segregated atomic configurations among which core/shell structures are particularly stable, in qualitative agreement with the experimental findings and calculations of smaller AgNi nanoalloys. Although binding energies demonstrate that these nanoalloys are thermodynamically stable independently of the composition, the excess energy indicates that only the formation of $Ag_{54}Ni$, $Ag_{48}Ni_7$ and $Ag_{42}Ni_{13}$ is favourable with respect to an ideal mixing of Ag_{55} and Ni_{55}. Among those, $Ag_{54}Ni$ and $Ag_{42}Ni_{13}$ are perfect core/shell configurations. $Ag_{26}Ni_{29}$ and $Ag_{23}Ni_{32}$ also exhibit marked minima of the excess energy. Those five stoichiometries also correspond to maxima of the second energy difference, so that they can be considered as magic compositions of the nanoalloy.

The magnetic phase diagram of these nanoalloys is complex. Contrary to what one would expect, the total moment of the nanoalloy in the high Ag concentration limit tends to decrease as increasing Ni concentration up to $Ag_{50}Ni_5$, due to the quenching of the Ni moment associated to the charge transfer from the outer 42 Ag atoms to the inner 13 ones. Beyond this Ni concentration, the total moment linearly increases as increasing Ni content up to $Ag_{18}Ni_{37}$, where a sudden drop of $9\mu_B$ takes place, to continue the linear increase with the same slope till the pure Ni limit. This linear increase is associated to the formation of a

sizable Ni subcluster with non quenched spin polarization and parallel magnetic couplings, being the contribution of the outer Ag atoms to the total moment of the nanoalloy negligible now. Therefore, the formation of a sizable Ni subcluster allows it to preserve its magnetic identity to a large extent when covered or interfaced by Ag, providing the nanoparticle with a magnetic moment localized in the core. The projected densities of states show that the HOMO rapidly acquires Ni character as increasing the Ni content. The clear Ni character of the HOMO for most stoichiometries indicates that, although the Ag-Ni interaction is weak and Ag provides a physical protection to the Ni core, Ni states should play an important role in the reactivity of these nanoalloys, as they indeed do in processes like ionization. The HOMO of the neutral cluster is of minority spin which explains why upon ionization the magnetic moment increases $1\mu_B$. The opposite happens upon an electron capture. Finally, many of the above magnetic trends have not an analog in the smaller nanoalloy of 13 atoms with the same icosahedral shape, a manifestation of the richness of behaviors at the nanoscale.

---

[1] T.B. Massalki, H. Okamoto and P.R. Subramanian, *Binary Alloy Phase Diagrams*, 2nd ed,; ASM International: Metals Park OH, 1990.

[2] F. Ducastelle, in *Order and Phase Stability in Alloys*, edited by R. de Boer and D.G. Pettifor, North Holland, Amsterdam, 1991.

[3] G. Mpourmpakis, G.E. Froudakis, A.N. Andriotis, and M. Menon, Role of Co in enhancing the magnetism of small Fe clusters, *Phys. Rev. B* 2005, **72**, 104417-104417-7.

[4] Anna N. Popova, Yuriy A. Zaharov and Valeri M. Pugachev, Chemical synthesis, structure and magnetic properties of nanocrystalline Fe-Co alloys, *Materials Letters*, 2012, **74**, 173-175.

[5] Andreas H$\acute{}$utten, Daniela Sudfeld, Inga Ennen, G$\acute{}$unter Reiss, Klaus Wojczykowski, and Peter Jutzi, Ferromagnetic FeCo nanoparticles for biotechnology. *J. Magn. Magn. Mater.*, 2005, **293**, 93-101.

[6] R. Ferrando, Julius Jellinek and R. L. Johnston, Nanoalloys: From theory to applications of alloy clusters and nanoparticles, *Chem. Rev.*, 2008, **108**, 845-910.

[7] O. Proulx, J. Regnard, I. Manzini, C. Revenant, B. Rodmacq and J. Mimault, In situ X-ray absorption spectroscopy study of the thermal behaviour of giant magnetoresistance Co_xAg_{1-x}

and Ni_xAg_{1-x} heterogeneous alloys, *Eur. Phys. J.: Appl. Phys.*, 2000, **9**, 115-124.

[8] Tetsuya O., Electrodeposition of highly functional thin films for magnetic recording devices of the next century, *Electrochimica Acta*, 2000, **45**, 3311-3321.

[9] Naeem A. M. Javed I. M., Najam-ul-Haq M., Hernandez G. P., Mahmood Q. A., Synthesis, magnetic and dielectric properties of Er-Ni doped Sr-hexaferrite nanomaterials for applications in High density recording media and microwave devices, *J. Magn. Magn. Mater.*, 2012, **324**, 15-19.

[10] Nelly M. Reilly, J. Ulises Reveles, Grant E. Johnson, Jorge M. del Campo, Shiv N. Khanna, Andreas M. Ko1ster, and A. W. Castleman, Jr., Experimental and theoretical study of the structure and reactivity of $Fe_mO_n^+$ $(m = 1 - 2;\ n = 1 - 5)$ with CO, *J. Phys. Chem. C*, 2007, **111**, 19086-19097.

[11] Nelly M. Reilly, J. Ulises Reveles, Grant E. Johnson, Shiv N. Khanna, and A. W. Castleman, Jr., Experimental and theoretical study of the structure and reactivity of $Fe_{1-2}O_{\leq 6}^-$ with CO, *J. Phys. Chem. A*, 2007, **111**, 4158-4166.

[12] Soumendu Datta and Badiur Rahaman, First principles study of electronic structure for cubane-like and ring-shaped structures of M_4O_4, M_4S_4 clusters (M = Fe, Co, Ni, Cu), *AIP ADVANCES*, 2015, **5**, 117231.

[13] A. Erlebach, C. Hühn, R. Jana and M. Sierka, Structure and magnetic properties of $(Fe_2O_3)_n$ clusters $(n = 1 - 5)$, *Phys. Chem. Chem. Phys.*, 2014 **16**, 26421-26426.

[14] H. Shiroishi, T. Oda, I. Hamada, and N. Fujima, Structure and magnetism on iron oxide clusters Fe_nO_m $(n = 1 - 5)$: Calculations from first principles, *Eur. Phys. J. D.*, 2003, **24**, 85-88.

[15] H. Shiroishi, T. Oda, I. Hamada, and N. Fujima, Structure and magnetism of anion iron oxide clusters $Fe_3O_m^-$ $(n = 3, 4)$, *Polyhedron*, 2005, **24**, 2472-2476.

[16] J.S. Kim, E. Kuk, K.N. Yu, J. Kim, S.J. Park, H.J. Lu, S.H. Kim, Y.K. Park, Antimicrobial effects of silver nanoparticles, *Nanomedicine: Nanotechnology, Biology and Medicine*, 2007, **3**, 95-101.

[17] M. Rail, A. Yadav, A. Gade, Silver nanoparticles as a new generation of antimicrobials, *Biotechnology Advances*, 2009, **27**, 76-83.

[18] M.A. Raza, Z. Kanwak, A. Rauf, A.N. Sabri, S. Riaz, and S. Nasseem, Size and shape dependent antibacterial studies of silver nanoparticles synthesized by wet chemical routes, *Nanomaterials*, 2016, **6**, 74-88.

[19] D. Poondi and J. Singh, Synthesis of metastable silver-nickel alloys by a novel laser-liquid-solid interaction technique, *J. Mater. Sci.*, 2000 **35**, 2467.

[20] Q. Xiao, Z. Yao, J. Liu, R. Hai, HY. Oderji and H. Ding, Synthesis and characterization of Ag-Ni bimetallic nanoparticles by laser induced plasma, *Thin Solid Films*, 2000 **519**, 7116-7119.

[21] Kalavathy Santhi, E. Thirumal, S.N. Karthick, Hee-Je Kim, Marimuthu Nidhin, V. Narayanan and A. Stephen, Synthesis, structure stability and magnetic properties of nanocrystalline Ag-Ni alloy, *J. Nanopart. Res.*, 2012, **14**, 868-875.

[22] H. Chiriac, M. Urse, F. Rusu, C. Hison and M. Neagu, Ni-Ag thin films as strain-sensitive materials for piezoresistive sensors, *Sensors and Actuators A: Physical*, 1999, **76**, 376-380.

[23] H-Y Chuang and D-H Chen, Fabrication and photocatalytic activities in visible and UV ligth regions of Ag@TiO_2 and NiAg@TiO_2, *Nanotechnology*, 2009, **20**(10), 105704-105713.

[24] H. Portales, L. Saviot, E. Duval, M. Gaudry, E. Cottancin, M. Pellarin, J. Lermé and M. Broyer, Resonant Raman scattering by quadrupolar vibrations of Ni-Ag core-shell nanoparticles, *Phys. Rev. B*, 2002, **65** 165422-165422-16.

[25] M. Gaudry, E. Cottancin, M. Pellarin, J. Lermé, L. Arnaud, J.R. Huntzinger, J.-L Vialle, M. Broyer, J.L. Rousset, M. Treilleux and P. Mélinon, Size and composition dependence in the optical properties of mixed (transition metal/noble metal) embedded clusters, *Phys. Rev. B*, 2003, **67**, 155409-155409-10.

[26] G. Rossi, A. Rapallo, C. Mottet, A. Fortunelli, F. Balleto and R. Ferrando, Magic polyicosahedral core-shell structures, *Phys. Rev. Lett.*, 2004, **93**, 105503 -105503-3.

[27] A. Rapallo, G. Rossi, R. Ferrando, A. Fortunelli, B.C. Curley, L.D. Lloyd, M. Tarbuck and R.L. Jonhston, Global optimization of bimetallic cluster structures.I. Size-mismatched Ag-Cu, Ag-Ni and Au-Cu systems, *J. Chem. Phys.*, 2005, **122**, 194308-194308-13.

[28] F. Calvo, E. Cottancin, and M. Broyer, Segregation, core alloying and shape transitions in bimetallic nanoclusters: Monte Carlo simulations, *Phys. Rev. B*, 2008, **77**, 121406-121406-4.

[29] M. Harb, F. Rabilloud and D. Simon, Structural, electronic, magnetic and optical properties of icosahedral silver-nickel nanoclusters, *Phys. Chem. Chem. Phys.*, 2010, **12**, 4246-4254.

[30] M. Harb, F. Rabilloud and D. Simon, Density functional study of structural and electronic properties of small bimetallic silver-nickel clusters, *J. Phys. Chem. A*, 2007, **111**, 7726-7731.

[31] D. Schooss, M.N. Blom, J.H. Parks, B. v. Issendorf, H. Haberland, and M.M. Kappes, The structures of Ag_{55}^{+} and Ag_{55}^{-}: Trapped ion electron difraction and Density Functional Theory,

NanoLett., 2005, **5**, 1972-1977.

[32] T. Rapps, R. Ahlrichs, E. Waldt, M. M. Kappes and D. Schooss, *Angew. Chem. Int. Ed.*, 2013, **52**, 6102-6105.

[33] Mauricio J. Piotrowski, Crina G. Ungureanu, Polina Tereshchuk, Krys E. A. Batista, Anderson S. Chaves, Diego Guedes-Sobrinho, and Juarez L. F. Da Silva, Theoretical study of the structural, energetic and electronic properties of 55-atom metal nanoclusters: A DFT investigation within van der Waals corrections, spin-orbit coupling, and PBE+U or 42 metal systems, *J. Phys. Chem. C*, 2016, **120**, 28844-28856.

[34] M. Pereiro, D. Baldomir, and J.E. Arias, Unexpected magnetism of small silver clusters, *Phys. Rev. A*, 2007, **75**, 063204-063204-4.

[35] Eva M. Fernández, José M. Soler, Ignacio L. Garzón, and Luis. C. Balbás, Trends in the structure and bonding of noble metal clusters, *Phys. Rev. B*, 2004, **70**, 165403-165403-14.

[36] **D. Bochicchio and R. Ferrando,** *Nano Letters***, 2010, 10, 4211-4216.**

[37] **D. Bochicchio and R. Ferrando,** *Phys. Rev. B***, 2013, 87, 165435-1-13.**

[38] **K. Laasonen, E. Panizon, D. Bochicchio, and R. Ferrando,** *J. Phys. Chem. C***, 2013, 117, 26405-26413.**

[39] J. M. Soler, E. Artacho, J. D. Gale, A. Garcí a, J. Junquera, P. Ordejón, and D. Sánchez-Portal, The SIESTA method for ab-initio order-N materials simulation, *J. Phys.: Condens. Matter.*, 2002, **14**, 2475-2486.

[40] J. P. Perdew, K. Burke, and M. Ernzerhof, Generalized gradient approximation made simple, *Phys. Rev. Lett.*, 1996, **77**, 3865-3868.

[41] N. Troullier, and J.L. Martins, Efficient pseudopotentials for plane-wave calculations, *Phys. Rev. B*, 1991, **43**, 1993-2006.

[42] L. Kleinman and D. M. Bylander, Efficacious form for model pseudopotentials, *Phys. Rev. Lett.*, 1982, **48**, 1425-1428.

[43] S. G. Louie, S. Froyen, and M. L. Cohen, Non linear ionic pseudopotentials in spin-density-functional calculations, *Phys. Rev. B*, 1982, **26**, 1738-1742.

[44] G. Kresse and J. Furthmüller, Efficient iterative schemes for *ab initio* total-energy calculations using a plane-wave basis set, *Phys. Rev. B*, 1996, **54**, 11169-11186.

[45] G. Kresse and J. Hafner, *Ab initio* molecular dynamics for liquid metals, *Phys. Rev. B*, 1993, **47**, R558-R561.

[46] Bader, R. F. W. *Atoms in Molecules. A Quantum Theory*; John Wiley and Sons, Ltd, Clarendon, Oxford, 1990.

[47] H. Henkelman, G.; Arnaldsson, A.; Jónsson, A fast and robust algorithm for Bader decomposition of charge density, *Comput. Mater. Sci.*, 2006, **36**, 354-360.

[48] A. Fortunelli and A. M. Velasco, Structural and electronic properties of Pt/Fe nanoclusters from EHT calculations, *J. Mol. Struc. (THEOCHEM)*, 1999, **487** , 251-266.

[49] **C. Mottet, G. Rossi, F. Baletto, and R. Ferrando,** *Phys. Rev. Lett*, **2005, 95, 035501-1-4.**

[50] F. Luis, F. Bartolomé, F. Petroff, J. Bartolomé, L.M. García, C. Deranholt, H. Jaffres, M.J. Martínez, P. Bencok, F. Wilhelm, A. Rogalev and N.B. Brookes, Tunning the magnetic anisotropy of Co nanoparticles by metal capping, *Europhys. Lett.*, 2006, **76**(1), 142-148.